Monthly Notices
of the
ROYAL ASTRONOMICAL SOCIETY

MNRAS **473,** 295–305 (2018)
Advance Access publication 2017 September 16

doi:10.1093/mnras/stx2384

Asteroid impacts on terrestrial planets: the effects of super-Earths and the role of the ν_6 resonance

Jeremy L. Smallwood,* Rebecca G. Martin, Stephen Lepp and Mario Livio

Department of Physics and Astronomy, University of Nevada, Las Vegas, 4505 South Maryland Parkway, Las Vegas, NV 89154, USA

Accepted 2017 September 8. Received 2017 September 8; in original form 2017 March 20

ABSTRACT

With *N*-body simulations of a planetary system with an asteroid belt, we investigate how the asteroid impact rate on the Earth is affected by the architecture of the planetary system. We find that the ν_6 secular resonance plays an important role in the asteroid collision rate with the Earth. Compared to exoplanetary systems, the Solar system is somewhat special in its lack of a super-Earth mass planet in the inner Solar system. We therefore first consider the effects of the presence of a super-Earth in the terrestrial planet region. We find a significant effect for super-Earths with a mass of around $10\,M_\oplus$ and a separation greater than about 0.7 au. For a super-Earth which is interior to the Earth's orbit, the number of asteroids colliding with Earth increases the closer the super-Earth is to the Earth's orbit. This is the result of multiple secular resonance locations causing more asteroids to be perturbed on to Earth-crossing orbits. When the super-Earth is placed exterior to Earth's orbit, the collision rate decreases substantially because the ν_6 resonance no longer exists in the asteroid belt region. We also find that changing the semimajor axis of Saturn leads to a significant decrease in the asteroid collision rate, though increasing its mass increases the collision rate. These results may have implications for the habitability of exoplanetary systems.

Key words: minor planets, asteroids: general – planets and satellites: dynamical evolution and stability.

1 INTRODUCTION

Asteroidal impacts on terrestrial planets may be important for planet habitability. Water must have been delivered to the surface of the Earth, potentially through asteroid impacts (Morbidelli et al. 2000; Raymond, Quinn & Lunine 2007; Izidoro et al. 2013), even though comet collisions and the interaction between the magma and atmosphere have also been suggested as sources of the planet's water (Lunine 2006; Genda & Ikoma 2008). Large moons may be produced through asteroid collisions (Canup & Asphaug 2001; Canup 2012). Our Moon plays an intricate role in the Earth's habitability by stabilizing the rotation axis of the Earth, preventing weather extremes due to chaotic motion. According to some hypotheses, life itself may have been delivered to Earth by asteroids (Cronin & Pizzarello 1983; Castillo-Rogez et al. 2008; Houtkooper 2011). Important heavy elements needed for the existence of life may have also been delivered by asteroid impacts (Willbold, Elliott & Moorbath 2011). The *rate* of asteroid impacts also can have a significant effect on a planet's habitability. A high rate of impacts could have led to a highly cratered planet, not hospitable to life. On the other hand, too few impacts could suppress the delivery of essential elements. The evolution of life on Earth shows that the presence of an asteroid belt could be necessary (e.g. through mass extinctions) even for the appearance of complex life and intelligence in an exosolar planetary system.

Asteroid belts, if they form at all, form most likely interior to giant planets (Morales et al. 2011; Martin & Livio 2013). This coincides with the location of the water snow line, the radius outside of which water is found in a solid form (Lecar et al. 2006). Giant planets form outside of the snow line and the terrestrial planets form inward of it (Raymond et al. 2009). While the gas disc is present, the eccentricities and inclinations of asteroids are damped by tidal interactions with the protoplanetary gas disc (Ward 1989, 1993; Artymowicz 1993; Agnor & Ward 2002; Kominami & Ida 2002). The lifetime of the gas disc is typically a few million years (Haisch, Lada & Lada 2001), after which photoevaporation disperses the disc. A pressure gradient arises when stellar radiation heats the disc, allowing the thermal energy of the gas to exceed its gravitational binding energy (Alexander, Clarke & Pringle 2006; Armitage 2010). Once the gas disc is removed, gravitational perturbations cause a clearing of asteroids at many resonance locations (Morbidelli et al. 1995; Gladman et al. 1997; Morbidelli & Gladman 1998; Petit, Morbidelli & Chambers 2001; Brož & Vokrouhlický 2008; Minton

* E-mail: smallj2@unlv.nevada.edu

& Malhotra 2010; Chrenko et al. 2015) leading to the formation of potential Earth impactors (Morbidelli & Nesvorný 1999; Strom et al. 2005).

Since Jupiter and Saturn are the largest planets in the Solar system, they are the main driving force for the dynamic evolution of the asteroid belt. The effect that Jupiter had on the asteroid collision rate on the Earth is debated (Horner & Jones 2008, 2012). The asteroid belt we observe today is roughly 0.1 per cent in mass of the original asteroid belt formed in the beginning of the Solar system. In a mean-motion resonance, the ratio of the orbital periods of two objects is an integer ratio (e.g. Armitage 2010). Several of the well-known mean-motion resonances in our Solar system are the Kirkwood gaps (Dermott & Murray 1983; Moons 1996; Vrbik 1996; O'Brien, Morbidelli & Bottke 2007), which are found within the asteroid belt. Secular resonances arise when the apsidal or nodal precession rates of two objects orbiting a central object are close (Yoshikawa 1987). For a review of the dynamics of secular resonances and mean-motion resonances, see Froeschle & Scholl (1986) and Moons (1996), respectively.

The most prevalent secular resonance in our Solar system in the ν_6 resonance (Ito & Malhotra 2006; Minton & Malhotra 2011), which occurs between the apsidal precession of the asteroids and Saturn. The outer edge of the ν_6 resonance location sets the inner boundary for our asteroid belt, which is approximately located at 2 au. A large fraction of near Earth asteroids originates from the inner main belt rather than the middle or outer belt (Bottke et al. 2002). Many of these asteroids within the inner main belt are injected in the ν_6 resonance and end up reaching Earth-crossing orbits (Morbidelli et al. 1994; Bottke, Rubincam & Burns 2000).

When asteroids encounter a resonance, their eccentricities are increased to a point where they are either ejected from the system or collide with a planet or the central star. These perturbations begin about 10^6 yr after the disc is dispersed (Morbidelli et al. 1994; Ito & Tanikawa 1999). Each resonance has a width, in semimajor axis, over which it operates (Dermott & Murray 1983). Asteroids that fall within the resonance width will undergo perturbations causing their eccentricities to increase. Regions in which the resonance widths overlap are known as chaotic regions (Murray & Holman 1997, 1999), and there almost all of the asteroids will be cleared out. The region where Jupiter's resonances overlap is what determines the outer edge of the asteroid belt at about 3.3 au.

The importance of the ν_6 resonance is apparent through observations of craters in the Solar system. The late heavy bombardment (LHB) event occurred early in the evolution of the Solar system. During this period, many lunar craters were formed from a large barrage of comets and asteroids. The LHB is assumed to have ended about 3.7–3.8 billion years ago. Bottke et al. (2012) found that the majority of these asteroids originated from the hypothetical extension of the asteroid belt, the E-belt, which was located between 1.7 and 2.1 au. This region underwent instabilities due to giant planet migration and is now depleted except for a family of high inclination asteroids.

Observations of exoplanetary systems show an abundance of systems which possess a super-Earth (Borucki et al. 2010, 2011; Batalha et al. 2013), a planet with a mass in the range of 1–10$M_\oplus$ (Valencia, Sasselov & O'Connell 2007). Fig. 1 shows the planet mass and semimajor axis of observed exoplanets. The area between the two black-dotted lines contains the observed super-Earths. The transparent yellow box denotes the observed super-Earths with a semimajor axis located at orbital radii in the range of the terrestrial planets in the Solar system. The vast majority of observed super-Earths are close to their parent star, although this is most likely

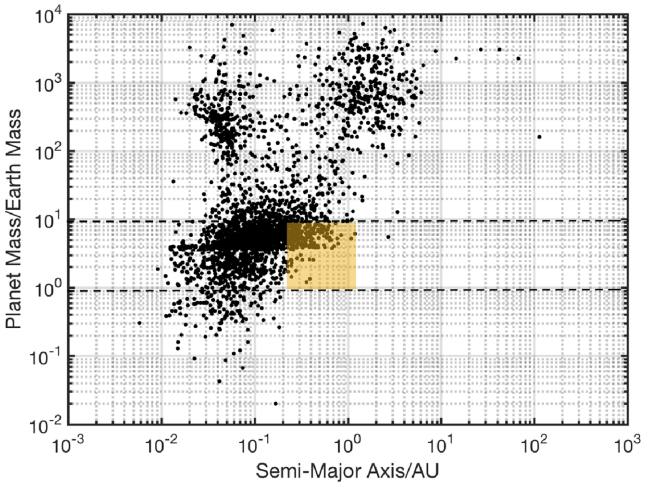

Figure 1. Planet mass and semimajor axis of observed exoplanets. The area between the two black-dotted lines contains the range of super-Earth masses ($1\,M_\oplus < M_p < 10\,M_\oplus$) used in simulations described in Section 2. The transparent yellow box denotes the observed super-Earths with a semimajor axis in the inner Solar system. The data are from exoplanets.org (Han et al. 2014).

a selection effect (Chiang & Laughlin 2013). In a recent work, Martin & Livio (2015) have shown that perhaps the main characteristic that distinguishes the Solar system from the observed exoplanetary systems is the absence of super-Earths. Consequently, it is very interesting to examine the effects that the presence of a super-Earth would have had on asteroid impacts on Earth. Since the evolution of a planetary system is a chaotic process (Malhotra 1999), adding a super-Earth can greatly influence the architecture of an exoplanetary system. There are likely additional mechanisms that operate in exoplanetary systems which result in the migration of planets, through the gas disc (Armitage 2010), through the planetesimal disc (Wyatt 2003; Gomes, Morbidelli & Levison 2004), via secular processes such as the Kozai–Lidov mechanism (Kozai 1962; Lidov 1962; Wu & Murray 2003; Takeda & Rasio 2005; Martin et al. 2016) and through planet–planet scattering (Ford & Rasio 2008; Dawson & Murray-Clay 2013). The *Kepler* data suggest that there is an overabundance of planetary systems with only one planet (Lissauer et al. 2011; Hansen & Murray 2013) and this may be due to the destructive motion of the planet (e.g. Morton & Winn 2014).

In this work, we are interested in multiplanet exoplanetary systems in which there has not been violent processes that might have destroyed an asteroid belt and prevented the formation of terrestrial planets early in the lifetime of the system. Specifically, we investigate how the architecture of the Solar system affects asteroid impacts on the Earth. In Section 2, we describe the *N*-body simulations that we use to model the evolution of an asteroid belt in a planetary system. In Section 3, we consider the effect of changing the structure of the inner Solar system. In particular, we examine the effect the presence of a super-Earth would have had. We find that the ν_6 resonance plays an important role in causing asteroid collisions with the Earth. In Section 4, we consider how the giant planets in the outer Solar system affect the location and strength of the ν_6 resonance. We draw our conclusions in Section 5.

2 *N*-BODY SIMULATIONS

We use the hybrid symplectic integrator in the orbital dynamics package, MERCURY, to model the structure of the asteroid belt and

the asteroid impact rate on the Earth in the presence of a super-Earth. MERCURY uses *N*-body integrations to calculate the orbital evolution of objects moving in the gravitational field of a large body (Chambers 1999). We simulate the motion of a super-Earth, Earth, Jupiter, Saturn and a distribution of asteroids orbiting a central object. The asteroids interact gravitationally with the planets and the star but do not interact with one another. We calculate the evolution of each asteroid orbit for a duration of ten million years.

The total mass observed in the Solar system's asteroid belt is about $5 \times 10^{-4} M_{\oplus}$, with about 80 per cent of the mass contained in the three largest asteroids (Ceres, Pallas and Vesta). Today, there are over 10 000 asteroids with high-accuracy measurements of the semimajor axis, with the mean being $<a> = 2.74 \pm 0.616$ au. The mean eccentricity is $<e> = 0.148 \pm 0.086$ and the mean inclination is $<i> = 8.^{\circ}58 \pm 6.^{\circ}62$ (Murray & Dermott 2000). However, the exact initial structure of the distribution of asteroids within an asteroid belt immediately after the dispersal of the protoplanetary disc is not fully understood. We assume that the asteroid distribution is sampled from a uniform distribution (Lecar & Franklin 1997). The semimajor axis of each asteroid is given by

$$a_{\rm i} = (a_{\rm max} - a_{\rm min}) \times \chi_r + a_{\rm min}, \quad (1)$$

where $a_{\rm min} = 1.558$ au is the inner boundary of the distribution, $a_{\rm max} = 4.138$ au is the outer boundary, and χ_r is a randomly generated number between 0 and 1. The inner and outer boundaries are determined using the structure of our own Solar system, $a_{\rm min}$ is three Hill radii beyond the semimajor axis of Mars and $a_{\rm max}$ is located at three Hill radii interior to Jupiter's orbit. The Hill radius is given by

$$R_{\rm H} = a_{\rm p} \left(\frac{M_{\rm planet}}{3 M_{\rm star}} \right)^{\frac{1}{3}} \quad (2)$$

where $a_{\rm p}$ is the semimajor axis of the planet and $M_{\rm planet}$ is the mass of the planet. Generally, three Hill radii is the planet's gravitational reach and thus no asteroids would likely be located within this region (Gladman 1993; Chatterjee et al. 2008; Morrison & Malhotra 2015).

The orbit of each asteroid is defined by six orbital elements, a, i, e, n, g and $M_{\rm a}$. The semimajor axis, a, is distributed uniformly in the range $a_{\rm min} < a < a_{\rm max}$, the inclination, i, is randomly allocated from the range 0°–10°, the eccentricity, e, is randomly generated from the range 0.0–0.1. The longitude of the ascending node, n, the argument of perihelion, g, and the mean anomaly, $M_{\rm a}$, are all uniformly randomly sampled from the range $0^{\circ} - 360^{\circ}$. The longitude of the ascending node, n, is defined as the angle from a reference direction to the ascending node, g is the angle from the ascending node to the object's periastron and $M_{\rm a}$ is the angular distance from the periastron. The present-day orbital elements for each of the planets are set as the initial parameters for the planets since the Solar system is stable over long time-scales (Duncan & Lissauer 1998; Ito & Tanikawa 2002).

The asteroids in our simulations are point particles that do not interact gravitationally with one another. We may neglect this interaction because the time-scale for asteroid–asteroid collisional interaction is much longer than the time-scale for the action of perturbations by resonance effects. The time-scale for resonant effects is on the order of ∼1 Myr, whereas some of the largest asteroids have collisional time-scales that are of the order of magnitude of the age of the Solar system (Dohnanyi 1969).

First, we checked the scalability of our results with the number of asteroids initially in the belt. We physically inflated the radius of the Earth to be 2×10^6 km, in order to enhance the number of asteroids on Earth-crossing orbits. We ran a simulation of Earth, Jupiter, Saturn and a uniformly distributed asteroid belt. The simulation ran for 10 Myr, with a timestep of 8 d with an accuracy parameter of 1×10^{-12}. The accuracy parameter measures approximately how much error per step the variable-timestep symplectic algorithm will tolerate. We ran three simulations with 10^3, 10^4 and 10^5 asteroids. We found that the number of asteroid collisions scaled linearly with the initial number of asteroids, as we would expect. Thus, to ensure faster simulation times and significant results we took the total number of asteroids in the rest of our work to be 10^4.

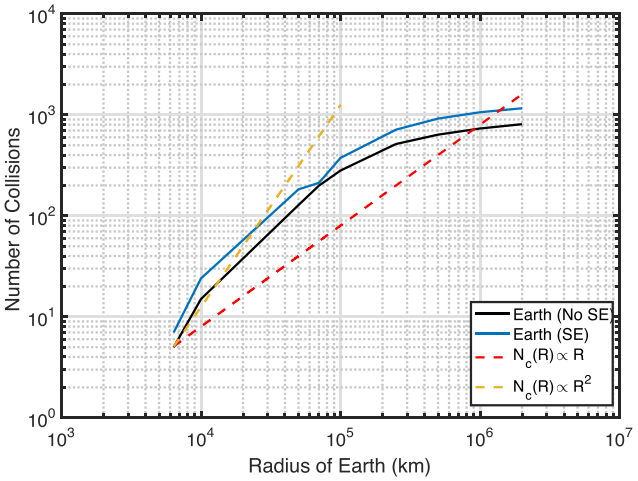

Figure 2. A log–log plot showing how the number of asteroid collisions scales with the inflated radius of the Earth, R. The black line shows how the total number of Earth collisions by asteroids ($N_{\rm c}$) scales with changing radius of our simulated inflated Earth. The blue lines shows the number of Earth collisions in the presence of a $10\,M_{\oplus}$ super-Earth at semimajor axis 0.8 au as a function of inflated Earth radii. The red-dotted line represents the line $N_{\rm c}(R) \propto R$ and the yellow-dotted line represents the line $N_{\rm c}(R) \propto R^2$.

Next, in Fig. 2, we examined how the number of asteroid collisions with the Earth scales with the radius of the inflated Earth. We ran two series of simulations which included Jupiter, Saturn, the asteroid belt and the inflated Earth. The first set does not include a super-Earth while the second set incorporated a super-Earth of mass $10\,{\rm M}_{\odot}$ at orbital separation 0.8 au. In each series of these simulations, we change the radius of the inflated Earth and measure the resulting asteroid collisions with the Earth. If the Earth has a radius of $1\,R_{\oplus}$ then the number of collisions throughout the simulation is only a few. The simulation with the super-Earth always produces a higher rate of collisions than the simulation without a super-Earth and so the effects of the super-Earth occur at all inflated-Earth radii. Thus, inflating the Earth allows for the detection of trends within the asteroid belt. In order to get statistically significant results, we inflated the size of the Earth to 2×10^6 km. Note that since the size of the Earth is inflated, we cannot compare the absolute numbers of asteroid collisions with the Earth with any other outcomes such as collisions with other planets or ejections. We are only able to compare the relative numbers of collisions with an object between simulations.

3 THE ARCHITECTURE OF THE INNER SOLAR SYSTEM

We first investigate the influence of the architecture of the inner Solar system on the asteroid collisions on Earth. In particular, since Martin & Livio (2015) identified the absence of super-Earths as

Table 1. Number of asteroidal outcomes for various simulated Solar system architectures involving a super-Earth (SE), Earth, Jupiter (J) and Saturn (S). Note that since the size of the Earth has been inflated, the number of Earth impacts cannot be compared to the other outcomes. We only make comparison between the number of Earth impacts between different simulations.

Simulation name	SE mass $M_\oplus$	SE semimajor axis au	Earth impacts	J/S/SE impacts	Star collision	Ejected	Remaining
run1	–	–	808	55	2	1112	8023
run2	5	0.22	803	42	1	1135	8019
run3	5	0.40	805	49	1	1121	8024
run4	5	0.50	826	45	3	1138	7988
run5	5	0.60	857	40	4	1115	7984
run6	5	0.70	877	47	1	1131	7944
run7	5	0.80	942	41	1	1121	7895
run8	5	1.20	394	51	1	1169	8385
run9	5	1.40	569	71	2	1221	8138
run10	10	0.22	798	63	1	1125	8013
run11	10	0.40	816	51	1	1122	8010
run12	10	0.50	874	53	3	1106	7964
run13	10	0.60	935	40	2	1118	7905
run14	10	0.70	978	32	2	1143	7845
run15	10	0.80	1236	43	3	1126	7592
run16	10	1.20	310	62	1	1166	8461
run17	10	1.40	615	77	1	1239	8068
run18	1	0.80	801	33	1	1157	8008
run19	2	0.80	843	58	2	1125	7972
run20	3	0.80	868	46	0	1147	7939
run21	4	0.80	913	52	5	1116	7914

perhaps the most important architectural element that distinguishes the Solar system from other exoplanetary systems, we vary the mass and semimajor axis of an additional super-Earth in the inner Solar system. The super-Earth's inclination and eccentricity are initially set to zero.

3.1 Total number of earth collisions

In Table 1, we show the parameters of 21 simulations and the summary of the asteroid collisional outcomes at a time of 10 Myr. We used super-Earth masses in the range 1–10 $M_\oplus$ and semimajor axis in the range 0.2–1.4 au. In each simulation, we determined the total number of asteroid impacts on the Earth, impacts on the other planets, impacts on the star, the number of asteroids ejected from the system and the number of asteroids remaining within the distribution. An asteroid is considered to have been ejected if its semimajor axis exceeds 100 au. Run1 from Table 1 represents our current Solar system as it includes Earth, Jupiter and Saturn but does not include a super-Earth planet. All of the simulations possessing a super-Earth were compared with that for our current Solar system. Since we have inflated the size of the Earth in order to enhance the number of collisions, we compare only collision rates with the Earth between simulations. We cannot compare the number of collisions with the Earth to the other outcomes of collisions with other bodies or ejections. We include the other outcomes only for completeness.

Fig. 3 shows the total number of asteroid collisions with the Earth (left-hand panel) and total number of collisions with the Earth as a function of super-Earth mass with an orbital separation of 0.8 au (right-hand panel) after a time of 10 Myr. A super-Earth which is located interior to Earth's orbit increases the asteroid impact rate on the Earth compared to a system without a super-Earth. A super-Earth located exterior to Earth's orbit, decreases the asteroid impact rate compared to a system without a super-Earth. A 10 $M_\oplus$ super-Earth located at a semimajor axis of 0.8 au causes the largest number of impacts on Earth, whereas a 10 $M_\oplus$ super-Earth located at a semimajor axis of 1.20 au causes the lowest rate of impacts on the Earth. There is a general trend for the total number of asteroid impacts on Earth for super-Earths located interior to Earth's orbit. As the separation of the super-Earth (from the Sun) increases, the asteroid impact flux on Earth also increases.

3.2 Evolution of the asteroid belt

Fig. 4 shows the evolution of the asteroid belt for simulations involving no super-Earth (top-left panel), a 10 $M_\oplus$ super-Earth at $a = 0.8$ au (top-right panel), a 10 $M_\oplus$ super-Earth at $a = 1.2$ au (bottom-left panel) and a 10 $M_\oplus$ super-Earth at $a = 1.4$ au (bottom-right panel). Each one of these systems also contains Earth, Jupiter and Saturn. The distribution was calculated every million years for 10 Myr. As the evolution takes place, areas of the asteroid distribution proceed to be cleared out by gravitational perturbations. These perturbations are the result of mean-motion and secular resonances with Jupiter and Saturn. The most notable mean-motion resonances are the 3:1, 5:2, 7:3 and 2:1, located at 2.5, 2.8, 2.9 and 3.3 au, respectively. These resonances are located at the same location as our Kirkwood Gaps. Jupiter's chaotic region is located at 3.6 au from the outer boundary of the asteroid distribution (4.133 au). This region is produced by overlapping widths of the mean-motion resonances (Murray & Holman 1997, 1999). The ν_6 resonance is located at 2.0 au along with Jupiter's 4:1 mean-motion resonance. The system containing a 10 $M_\oplus$ super-Earth located at a semimajor axis of 0.8 au appears to have a broader ν_6 width than a system with no super-Earth. In contrast, if the super-Earth is located exterior to Earth's orbit, the ν_6 resonance completely disappears. We discuss this further in Sections 3.3 and 3.5.

3.3 Resonances in the asteroid belt

There are five potential outcomes for each asteroid during the various simulations. These are: ejection of the asteroid from

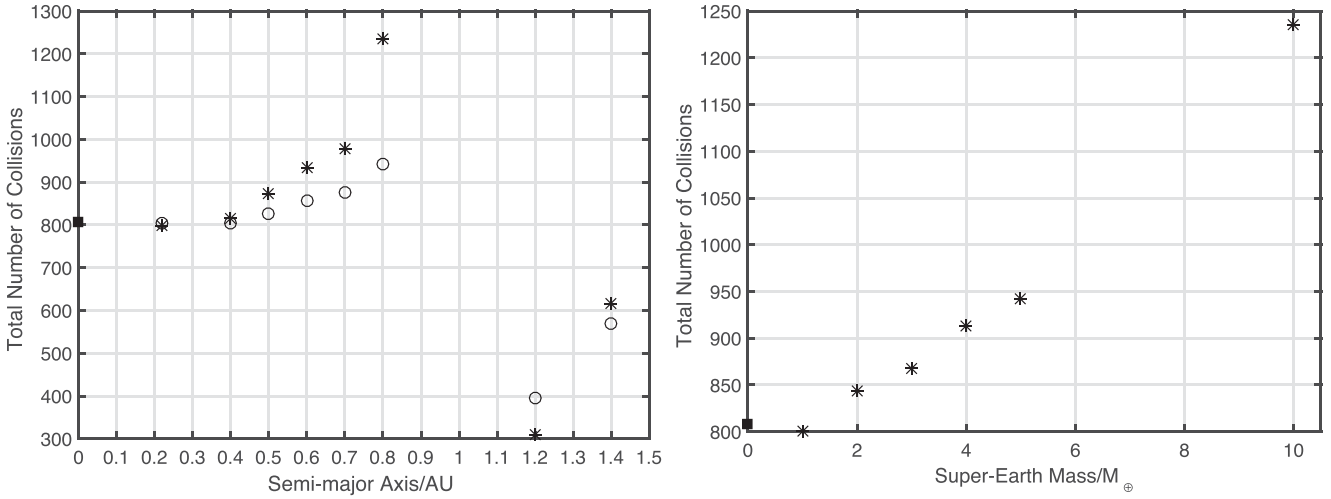

Figure 3. Left-hand panel:total number of asteroid collisions with the Earth as a function of the semimajor axis of the super-Earth. The simulations with a $5M_{\oplus}$ super-Earth are denoted by hollow circles and the simulations with a $10M_{\oplus}$ super-Earth are represented by the star symbols. The square represents the simulation of the standard Solar system (without a super-Earth). Right-hand panel: total number of asteroid collisions with the Earth as a function of super-Earth mass in units of Earth masses ($M_{\oplus}$) at semimajor axis $a_{\rm SE} = 0.8$ au.

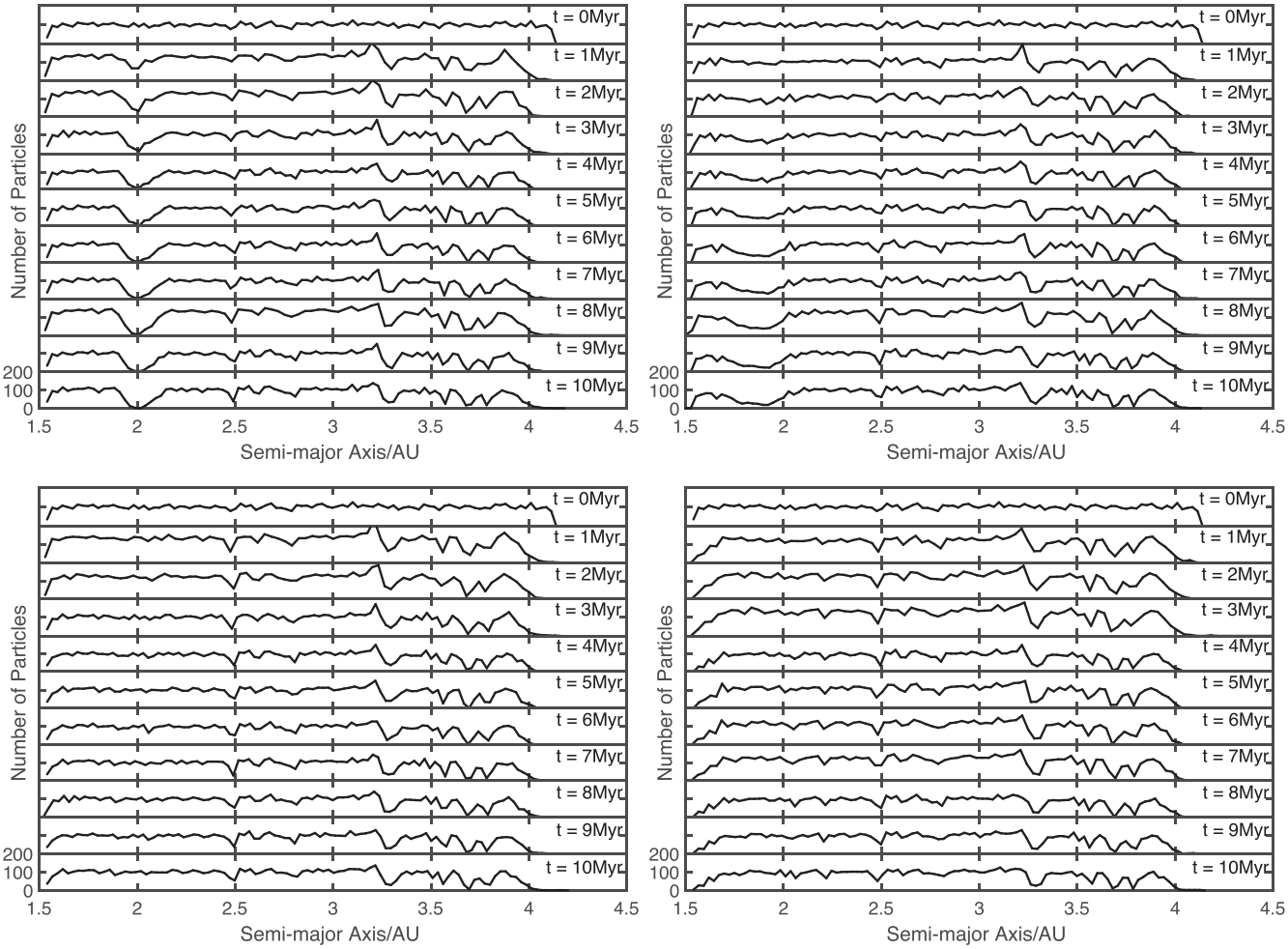

Figure 4. Evolution of the asteroid distribution over a span of 10 million years. The asteroid distribution is located in a system containing Earth, Jupiter, Saturn and a super-Earth (except for the control simulation at top left). The asteroids are initially sampled from a uniform distribution in semimajor axis values, represented at $t = 0$ Myr. Top-left panel: evolution of asteroid distribution without a super-Earth. Top-right panel: evolution of asteroid distribution with a $10M_{\oplus}$ super-Earth located at a semimajor axis of 0.8 au. Bottom-left panel: evolution of asteroid distribution with a $10M_{\oplus}$ super-Earth located at 1.2 au. Bottom-right panel: evolution of asteroid distribution with a $10M_{\oplus}$ super-Earth located at 1.4 au.

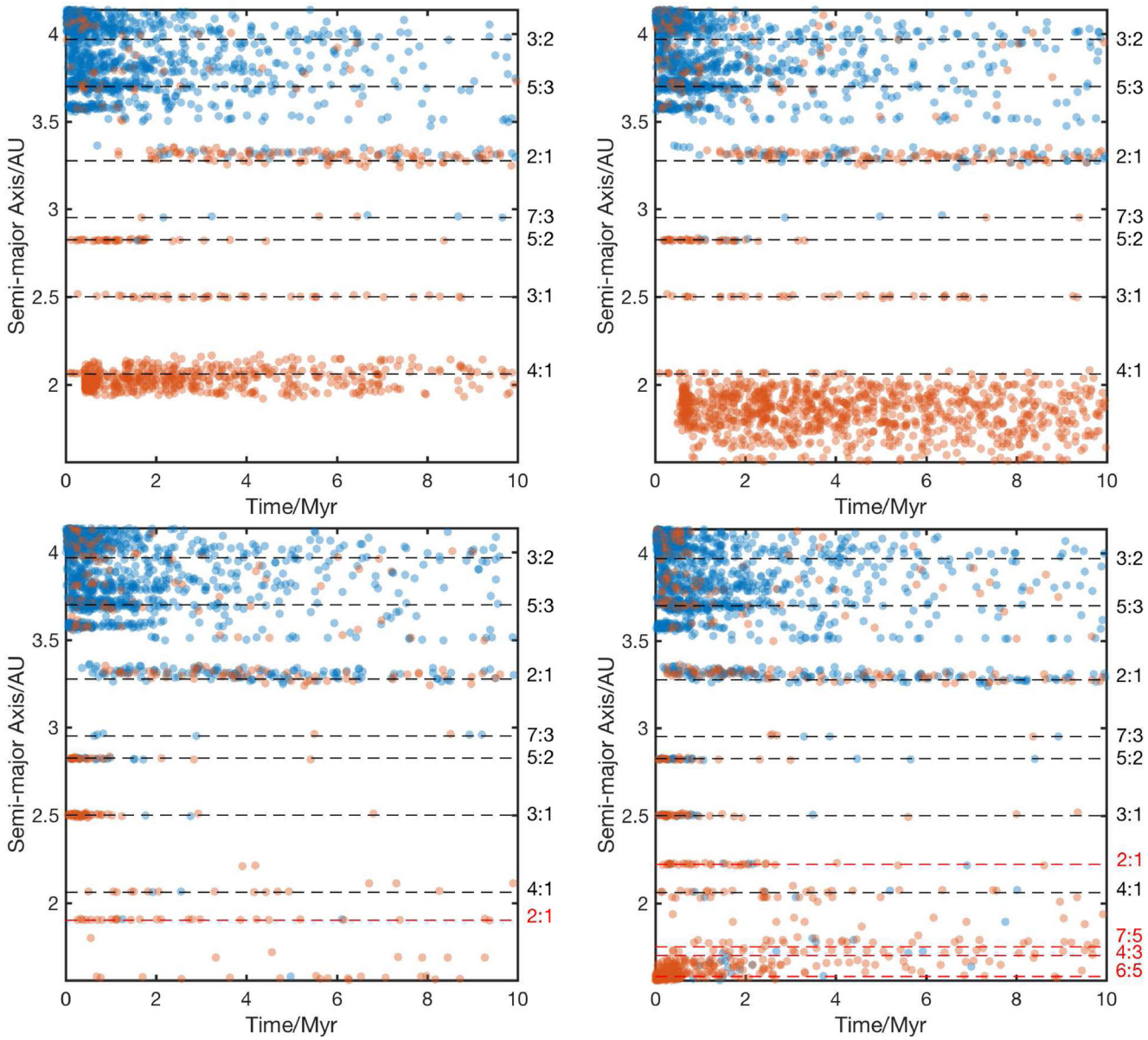

Figure 5. The original semimajor axis of each asteroid as a function of the time when the final outcome occurred. The possible outcomes for each asteroid include Earth-impact (red) and other (blue). 'Other' refers to ejection, super-Earth impact, Jupiter-impact, Saturn-impact or colliding with the central object. The inner and outer boundaries of the asteroid distribution are located at $a_{\rm min} = 1.558$ au and $a_{\rm max} = 4.138$ au. Top-left panel: asteroid outcomes for a system with no super-Earth. Top-right panel: 10 $M_\oplus$ super-Earth located at a semimajor axis of 0.8 au. Bottom-left panel: 10 $M_\oplus$ super-Earth located at a semimajor axis of 1.2 au. Bottom-right panel: 10 $M_\oplus$ super-Earth located at a semimajor axis of 1.4 au. The mean-motion resonances with Jupiter are represented with the black-dotted line, with the name of each resonance listed to the right of their respected line. The mean-motion resonances with the super-Earth are represented by the red-dotted lines.

the Solar system, collision with the Earth, collision with another planet, collision with the Sun or the asteroid remaining in the asteroid belt. Fig. 5 shows the various asteroid outcomes for a system with no super-Earth (top-left panel), a 10 $M_\oplus$ super-Earth located at a semimajor axis $a = 0.8$ au (top-right panel), a 10 $M_\oplus$ super-Earth located at $a = 1.2$ au (bottom-left panel) and a 10 $M_\oplus$ super-Earth located at $a = 1.4$ au (bottom-right panel). The initial semimajor axis of each asteroid is shown as a function of the time of its final outcome. The asteroids which were cleared out are originally located at the resonance locations, because mean-motion and secular resonances operate over the initial semimajor axis of each asteroid, increasing the asteroid's eccentricity. On the right hand vertical axis, we show the mean-motion resonance locations with Jupiter and the super-Earth. When a 10 $M_\oplus$ super-Earth is located at $a = 0.8$ au, there is a widening of the ν_6 secular resonance, which increases the number of asteroids perturbed on to Earth-colliding orbits. When the super-Earth is placed exterior to Earth's orbit, there is a substantial decrease in the number of Earth-colliding asteroids. This is due to the ν_6 resonance being suppressed. When the super-Earth is located exterior to Earth's orbit, a 2:1 mean-motion resonance is created within the asteroid belt. This resonance causes additional asteroids to be cleared out. A chaotic zone, due to the super-Earth, is seen for the system with a $10M_\oplus$ super-Earth located at 1.4 au. This chaotic zone is produced from the overlapping libration widths

of the super-Earth's 6:5, 4:3 and 7:5 mean-motion resonances. This chaotic zone causes a larger number of asteroids to be cleared out from the inner parts of the asteroid belt.

3.4 Collision rate on the earth

To determine the frequency of asteroid collisions with the Earth, the asteroid collision rate was calculated and plotted in Fig. 6. In the top panel, we show the collision rate for systems with a $10\,M_\oplus$ super-Earth at various semimajor axis locations and in the bottom panel, the collision rate for systems with a $5\,M_\oplus$ super-Earth for various semimajor axis values. The collision rate was calculated per million years, for 10 Myr. Initially, the collision rate is higher than compared to later times, due to the fact that there is a larger asteroid population at the beginning of the simulations than at the end. After 1 Myr, the super-Earth located at 1.4 au caused the greatest number of collisions, but the rate rapidly declined. This behaviour is due to the chaotic region of the super-Earth, which quickly clears out asteroids in locations of overlapping resonances, perturbing them on to Earth-crossing orbits. This chaotic region can be clearly seen in the bottom-right panel in Fig. 5. The system with a $10\,M_\oplus$ super-Earth at 0.8au has the highest asteroid impact rate for the duration of the simulation. When comparing with the simulations that involve $5\,M_\oplus$ super-Earths, the collision rate is also the highest for a super-Earth located at $a = 0.8$ au.

3.5 The ν_6 resonance

As shown in Fig. 5, the majority of the asteroid collisions with the Earth are from asteroids that originate from the location of the ν_6 resonance in the asteroid belt (see also Morbidelli et al. 1994; Gladman et al. 1997; Bottke et al. 2000; Minton & Malhotra 2011; Haghighipour & Winter 2016). Thus, this secular resonance may have played a significant role in making the Earth habitable. In our simulation without a super-Earth, the total number of asteroids that collided with the Earth from secular resonances was about two and a half times that from mean-motion resonances.

The ν_6 secular resonance is due to both Saturn and Jupiter. Jupiter increases the precession frequency of the asteroids so that they fall into a resonance with the apsidal precession rate of Saturn. In Fig. 7, we show the precession rate of a test particle as a function of orbital separation. The solid horizontal line denotes the g_6 eigenfrequency of Saturn which is found by calculating the eigenvalues of the matrix A_{ij} associated with a generalized form of the secular perturbation theory (see, e.g. section 7.7 in Murray & Dermott 2000). The top-left and top-right correspond to the systems which include no super-Earth and a super-Earth located interior to Earth, respectively, and the bottom-left and bottom-right both correspond to systems with a super-Earth located exterior to Earth. The values of Saturn's eigenfrequency for each of these systems are found to be 22.13, 22.15, 22.18 and 22.20 arcsec yr^{-1}, respectively. The inclusion of a super-Earth has little influence on the value of the g_6 eigenfrequency. We also find that the inclusion of Saturn does not noticeably affect the precession rate of the asteroids – that rate is dominated by Jupiter. The top-left panel of Fig. 7 resembles our Solar system with the inclusion of Earth, Jupiter, Saturn and the asteroid belt. The intersection of the particle's precession rate with Saturn's eigenfrequency represents the location of the ν_6 resonance, which is located at ∼2 au.

The inclusion of a super-Earth, which has a mass that is significantly smaller than that of the giant planets, Jupiter and Saturn, can lead to a change in the asteroid precession rate large enough

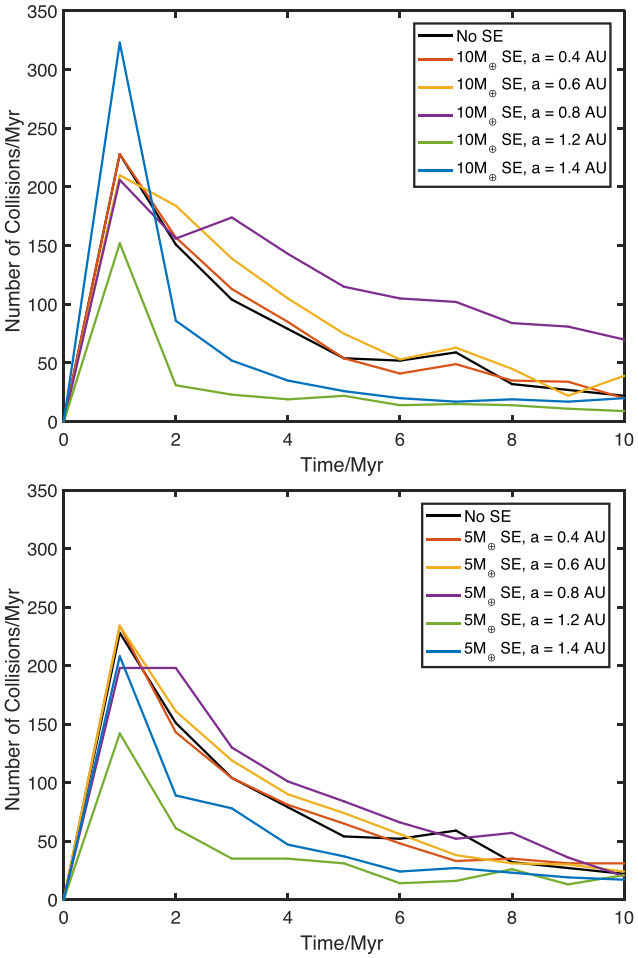

Figure 6. Number of asteroid collisions towards Earth per million year for selected simulations described in Table 1. Top panel: collision rate for simulations involving a $10M_\oplus$ super-Earth. Bottom panel: collision rate for simulations involving a $5M_\oplus$ super-Earth.

to enhance or to remove the resonance with Saturn, depending on the location and mass of the super-Earth. The enhancement of the ν_6 resonance is observed in the top-right panel of Fig. 7, where the super-Earth is located interior to Earth's orbit at a semimajor axis $a = 0.80$ au. The precession rate of the test particle is close to the eigenfrequency of Saturn for semimajor axis values from ∼1.5 au to ∼2 au, which causes an enhancement of the ν_6 resonance.

Re-examining the top-left panel in Fig. 7, there are two ν_6 resonance locations, located at about 1.3 au and 2.0 au, respectively. When a super-Earth is included within this model at an orbital separation of 0.8 au, these two resonance locations become closer together as the mass of the super-Earth increases. We follow Malhotra (2012) by constructing an analytical toy model of the ν_6 resonance width by calculating the forced maximum eccentricity of a test particle near the ν_6 resonance with and without a super-Earth. When the mass of the super-Earth reaches $10\,M_\oplus$, the widths of the two ν_6 resonances overlap and the resonance operates over a larger range of semimajor axis values.

The removal of the ν_6 resonance occurs when the super-Earth is located exterior to Earth's orbit. This can be seen in the bottom-left panel (super-Earth located at $a = 1.2$ au) and the bottom-right panel (super-Earth located at $a = 1.5$ au) of Fig. 7, where the precession

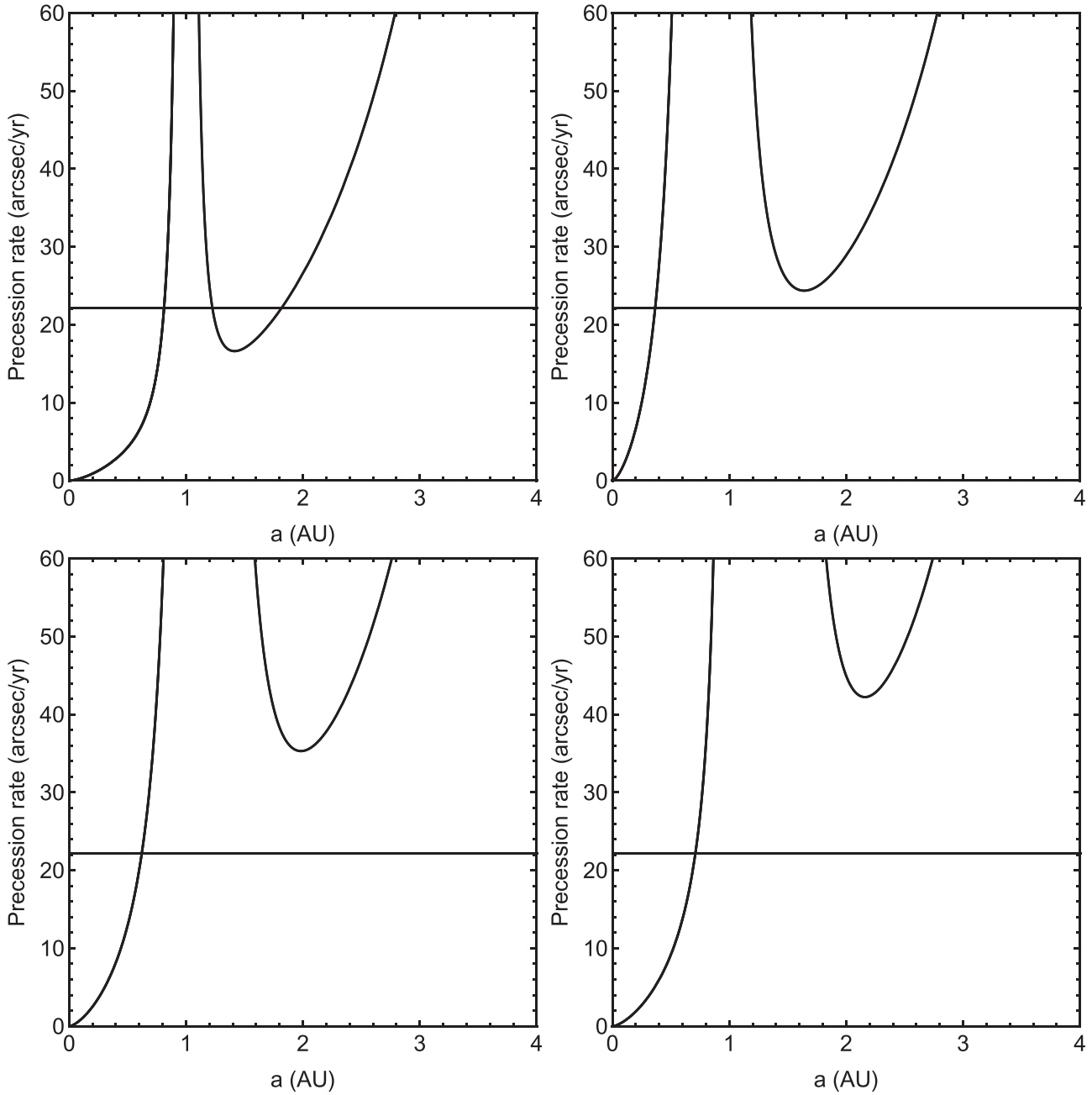

Figure 7. The precession rate of a test particle as a function of semimajor axis in the inner part of the Solar system. The solid horizontal line represents the g_6 eigenfrequency of Saturn. The intersection of the precession rate of the test particle with the eigenfrequency of Saturn denotes the location of a secular resonance. Top-left panel: a system with no super-Earth. In this case, the intersection located at 2 au is the location of the ν_6 resonance within the asteroid belt. Top-right panel: a system with a $10\,M_\oplus$ super-Earth located at a semimajor axis of $a = 0.8$ au. Bottom-left panel: a system with a $10\,M_\oplus$ super-Earth located at a semimajor axis of $a = 1.2$ au. Bottom-right panel: a system with a $10\,M_\oplus$ super-Earth located at a semimajor axis of $a = 1.4$ au.

rate of the test particle does not intersect with the eigenfrequency of Saturn, leading to the disappearance of the ν_6 resonance. This analysis of the precession rate of a test particle agrees with the results described in the previous section. Re-examining Fig. 5, we can see that when the super-Earth is located interior to Earth's orbit we have a widening of the width ($\sim$1.5 to $\sim$2.0 au) of the ν_6 resonance, whereas if the super-Earth is located exterior to Earth's orbit, the resonance is removed. Thus, the enhancement or removal of the ν_6 resonance is predicated on the location and mass of the super-Earth.

4 THE ARCHITECTURE OF THE OUTER SOLAR SYSTEM

We next considered the properties of the outer giant planets which produce a ν_6 resonance in the location of the asteroid belt. We keep the mass and orbital separation of Jupiter fixed. The location of the ν_6 resonance as a function of Saturn's semimajor axis and mass is shown in Fig. 8. In the left-hand panel, the location of the ν_6 resonance as a function of Saturn's semimajor axis was found by calculating the resulting eigenfrequency of Saturn and then finding

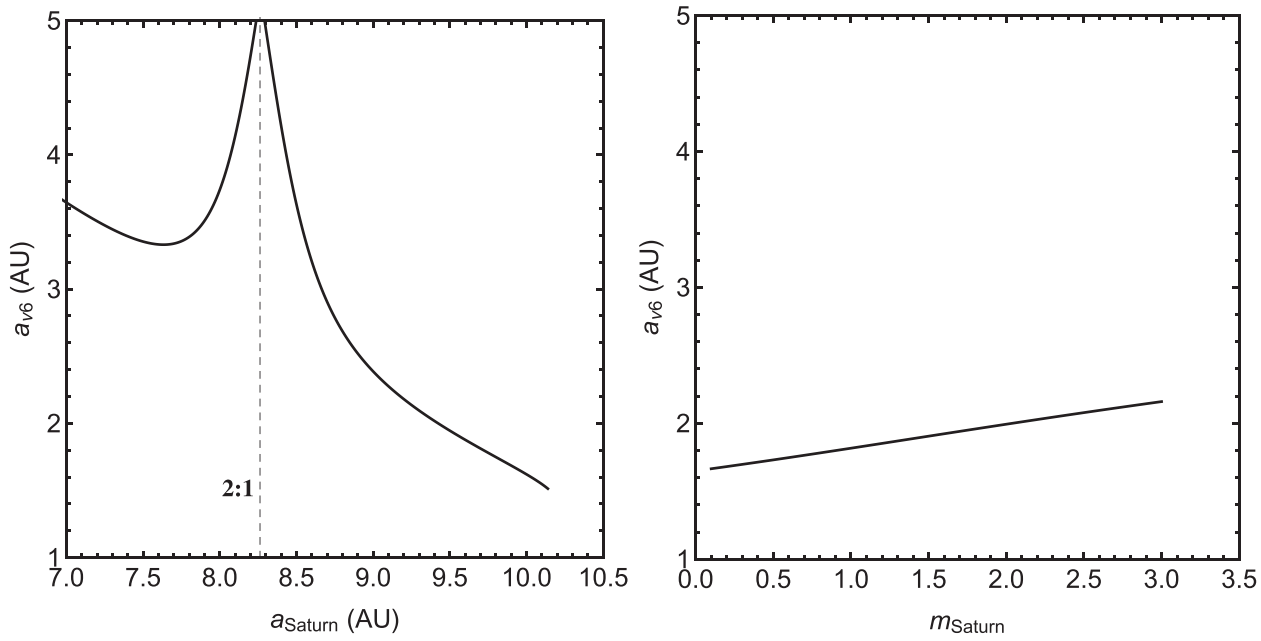

Figure 8. Left-hand panel:location of the ν_6 secular resonance with respect to the semimajor axis of Saturn. We have included a correction due to the 2:1 mean-motion resonance between Jupiter and Saturn (Malhotra et al. 1989; Minton & Malhotra 2011). The dotted line shows the location of this 2:1 mean-motion resonance. Right-hand panel: location of the ν_6 resonance as a function of the mass of Saturn.

Table 2. Number of asteroidal outcomes with varying parameters of Saturn. Each simulation includes Earth, Jupiter (J) and Saturn (S). Note that since the size of the Earth has been inflated, the number of Earth impacts cannot be compared to the other outcomes. We only make comparison between the number of Earth impacts between different simulations.

Simulation name	Saturn mass M_S	Saturn semimajor axis au	Earth impacts	J/S impacts	Star collision	Ejected	Remaining
run22	1.0	8.0	514	113	2	2705	6666
run23	1.0	9.0	1012	37	0	1206	7745
run24	1.0	9.537	808	55	2	1112	8023
run25	1.0	10.0	957	48	4	1034	7957
run26	1.0	11.0	248	50	1	966	8735
run27	1.0	12.0	210	54	1	928	8807
run28	0.1	9.537	172	83	1	874	8870
run29	0.5	9.537	447	55	2	1005	8491
run30	1.0	9.537	808	55	2	1112	8023
run31	1.5	9.537	1163	49	3	1238	7547

the location of the intersection with the precession rate of a test particle. The precession frequency of the test particle was calculated by including the planets, Earth, Jupiter and Saturn. However, Saturn's eigenfrequency was calculated by including only Jupiter since the Earth has a negligible influence in the calculation. We included a correction due to the near 2:1 mean-motion resonance between Jupiter and Saturn (Malhotra et al. 1989; Minton & Malhotra 2011). The location of the resonance drastically moves outwards as Saturn becomes closer to a 2:1 resonance with Jupiter at about 8.3 au. As Saturn moves outwards, the resonance location moves inwards. The right-hand panel of Fig. 8 shows the location of the ν_6 resonance as a function of Saturn's mass, while Saturn is located at its current semimajor axis of 9.5 au. We direct the readers to a more accurate calculation of Minton & Malhotra (2011)(see their fig. 2) for the value of g_6 and the ν_6 location as a function of Saturn's semimajor axis. If we increase Saturn's mass, then the location of the resonance moves outwards slightly. For a mass which is one-tenth of its current value, the resonance moves inwards only slightly. The resonance location is rather more sensitive to the orbital separation than to the mass of Saturn.

We have run additional numerical simulations of the asteroid belt to consider the effects of varying the properties of the outer giant planets. We varied Saturn's semimajor axis and mass to verify the trends found in Fig. 8. The results of these simulations are presented in Table 2. Varying Saturn's semimajor axis (runs 22–27 from Table 2) follows the trend calculated in Fig. 8 (left-hand panel). As Saturn's semimajor axis increases, the location of the ν_6 resonance moves outside the asteroid belt boundaries. On the other hand, when the semimajor axis decreases, the ν_6 resonance moves towards the middle/outer regions of the asteroid belt. This change in the location of the resonance can be seen in Fig. 9, where the left-hand panel represents the various asteroid outcomes when Saturn is located at a semimajor axis of $a = 8.0$ au and the right-hand panel shows the outcomes for when Saturn is located at $a = 12.0$ au. Again, the time of the particular outcome is plotted with respect to the initial semimajor axis of each asteroid.

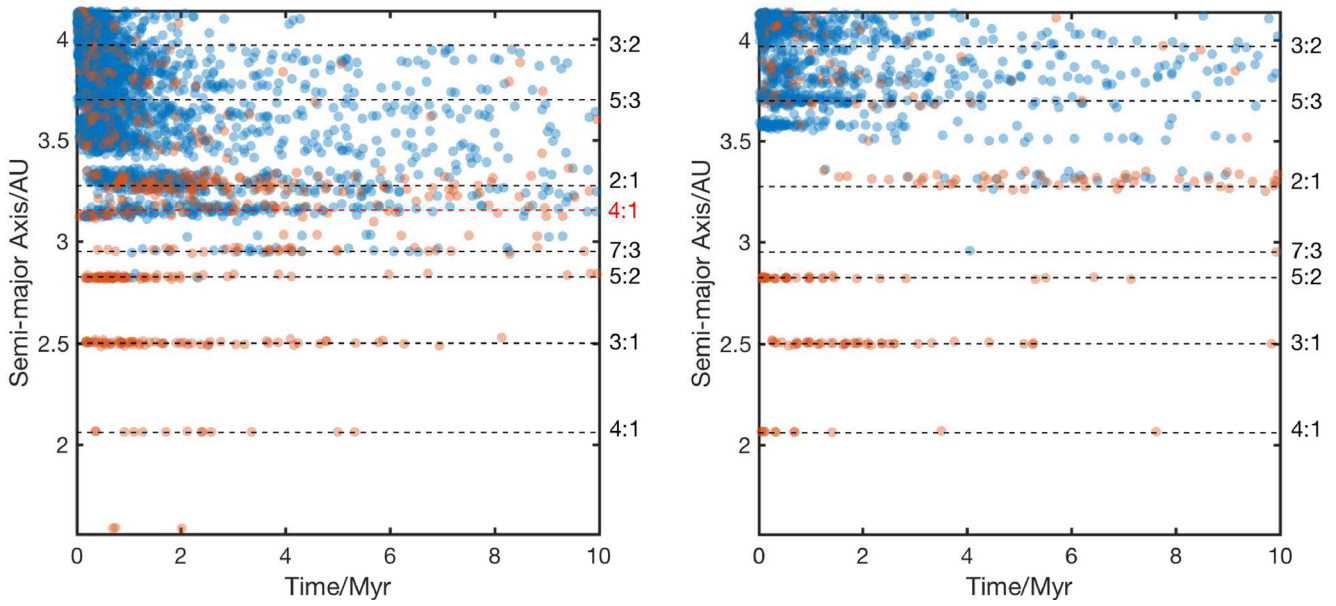

Figure 9. The original semimajor axis of each asteroid as a function of the time when the final outcome occurred. The possible outcomes for each asteroid include Earth-impact (red) and other (blue). 'Other' refers to ejection, Jupiter-impact, Saturn-impact or colliding with central object. The inner and outer boundary of the asteroid distribution are located at $a_{\rm min} = 1.558$ au and $a_{\rm max} = 4.138$ au. Left-hand panel: asteroid outcomes for a system with Saturn located at a semimajor axis $a = 8$ au. Right-hand panel: Saturn located at a semimajor axis $a = 12$ au. The mean-motion resonances with Jupiter are represented with the black-dotted line and the red-dotted line represents a mean-motion resonance between the asteroids and Saturn. Each mean-motion resonance is listed to the right of their respected line.

For the case where Saturn is located at $a = 8.0$ au, the location of the ν_6 resonance is shifted outwards to approximately 3.5 au, which is what is expected according to the left-hand panel of Fig. 8. This movement of the resonance causes a decrease in the number of collisions with the Earth, but causes a significant increase in the number of asteroid ejections. For the situation where Saturn's semimajor axis is taken to be 12.0 au, there is no ν_6 secular resonance. The disappearance of the resonance is caused by there being no intersection of the particles precession rate with Saturn's eigenfrequency. Overall we find that varying the orbital separation of Saturn in both directions has a significant effect on the location of the ν_6 secular resonance and that it generally leads to a decrease in the number of asteroid collisions. However, the orbital location of Saturn may not be accidental, since it is close to being in the 5:2 resonance with Jupiter. Fernández & Ip (1984, 1996) suggested the jovian planets proximity to the current near resonant structure could be a consequence of the differential expansion of their orbits during late stages of planetary formation (e.g. Michtchenko & Ferraz-Mello 2001).

When the mass of Saturn is changed (runs 28–31 from Table 2), the calculated trend in Fig. 8 (right-hand panel) breaks down for masses greater than 1.5 $M_{\rm Saturn}$ (results not shown in Table 2). For the situations where Saturn's mass is greater than 1.5 $M_{\rm Saturn}$, the Earth's orbit becomes highly eccentric ($e \approx 0.5$) which causes a higher number of asteroid impacts. When Saturn has a mass of 0.1 $M_{\rm Saturn}$, the number of asteroid collisions with Earth is substantially lower, since the ν_6 resonance is located outside the asteroid distribution. The location of the ν_6 resonance is more sensitive to changes in Saturn's orbital separation than to its mass.

5 CONCLUSIONS

We found that the ν_6 resonance may play an important role in producing asteroid collisions with terrestrial planets in the inner parts of a planetary system (see also Morbidelli et al. 1994; Gladman et al. 1997; Bottke et al. 2000; Ito & Malhotra 2006). Using *N*-body simulations and analytical models we have modelled planetary systems with terrestrial planets, an asteroid belt and two giant planets, in this order in terms of their separation from the central star. We have explored how the planetary system architecture affects the location and width of the ν_6 resonance and how this in turn affects the number of asteroid collisions with the Earth. Since super-Earths are common in the inner regions of exoplanetary systems we first considered their influence. A super-Earth with a mass of around 10 $M_\oplus$ at an orbital radius greater than about 0.7 au may significantly affect the number and rate of asteroid collisions on the Earth. A super-Earth interior to the Earth's orbit increases the number of asteroid collisions with the Earth, while a super-Earth between the Earth and the asteroid belt decreases the number of asteroid collisions. Furthermore, we find that increasing the mass of Saturn increases the number of asteroid collisions. Changing the location of Saturn generally leads to a significant decrease in the number of asteroid collisions. The slight differences between our numerical calculations and analytical models were due to neglecting higher-order terms within our analytical models.

Schlichting, Warren & Yin (2012) proposed that additional collisions from a residual planetesimal population are needed to damp the high eccentricities and inclinations of terrestrial planets during the late stages of planet formation. This damping mechanism would allow terrestrial planets to evolve on to circular and coplanar orbits. Geochemical evidence suggests that the Earth accreted roughly 0.3 per cent–0.7 per cent of its total mass in the form of chondritic material during the late stages of planet formation (Walker 2009). If these series of events are indeed true, this implies that asteroid collisions may have an important effect on determining the habitability of planets located in exoplanetary systems, which would make the results in this work potentially very significant. In particular, and to end on a speculative note, Martin & Livio (2016) proposed a model in which super-Earths did form in the inner parts of

the Solar system, but then migrated into the Sun. Since we have shown that the rate of asteroid impacts on Earth is affected by the presence (or not) of an inner super-Earth, this chain of events, if it had indeed happened, surely had an effect on both the rate and pattern of asteroid impacts. It is tempting to speculate, therefore, that the resulting pattern and rate may have made the Earth more conducive to the emergence and evolution of life.

ACKNOWLEDGEMENTS

We thank an anonymous referee for valuable comments that improved the quality of our manuscript. All the simulations ran at the UNLV National Supercomputing Institute on the Cherry Creek cluster. This research made use of the Exoplanet Orbit Database and the Exoplanet Data Explorer at exoplanets.org. We acknowledge support from NASA through grant NNX17AB96G. JLS also acknowledges support from a graduate fellowship from the Nevada Space Grant Consortium (NVSGC).

REFERENCES

Agnor C. B., Ward W. R., 2002, ApJ, 567, 579
Alexander R. D., Clarke C. J., Pringle J. E., 2006, MNRAS, 369, 229
Armitage P. J., 2010, Astrophysics of Planet Formation, Cambridge Univ. Press, Cambridge, p. 294
Artymowicz P., 1993, ApJ, 419, 166
Batalha N. M. et al., 2013, ApJS, 204, 24
Borucki W. J. et al., 2010, Science, 327, 977
Borucki W. J. et al., 2011, ApJ, 736, 19
Bottke W. F., Jr, Rubincam D. P., Burns J. A., 2000, Icarus, 145, 301
Bottke W. F., Morbidelli A., Jedicke R., Petit J.-M., Levison H. F., Michel P., Metcalfe T. S., 2002, Icarus, 156, 399
Bottke W. F., Vokrouhlický D., Minton D., Nesvorný D., Morbidelli A., Brasser R., Simonson B., Levison H. F., 2012, Nature, 485, 78
Brož M., Vokrouhlický D., 2008, MNRAS, 390, 715
Canup R. M., 2012, Science, 338, 1052
Canup R. M., Asphaug E., 2001, Nature, 412, 708
Castillo-Rogez J. C., Matson D. L., Kargel J. S., Vance S. D., Johnson T. V., 2008, LPS, 39, 1391
Chambers J. E., 1999, MNRAS, 304, 793
Chatterjee S., Ford E. B., Matsumura S., Rasio F. A., 2008, ApJ, 686, 580
Chiang E., Laughlin G., 2013, MNRAS, 431, 3444
Chrenko O., Brož M., Nesvorný D., Tsiganis K., Skoulidou D. K., 2015, MNRAS, 451, 2399
Cronin J. R., Pizzarello S., 1983, Adv. Space Res., 3, 5
Dawson R. I., Murray-Clay R. A., 2013, ApJ, 767, L24
Dermott S. F., Murray C. D., 1983, Nature, 301, 201
Dohnanyi J. S., 1969, J. Geophys. Res., 74, 2531
Duncan M. J., Lissauer J. J., 1998, Icarus, 134, 303
Fernández J. A., Ip W.-H., 1984, Icarus, 58, 109
Fernández J. A., Ip W.-H., 1996, Planet. Space Sci., 44, 431
Ford E. B., Rasio F. A., 2008, ApJ, 686, 621
Froeschle C., Scholl H., 1986, A&A, 166, 326
Genda H., Ikoma M., 2008, Icarus, 194, 42
Gladman B., 1993, Icarus, 106, 247
Gladman B. J. et al., 1997, Science, 277, 197
Gomes R. S., Morbidelli A., Levison H. F., 2004, Icarus, 170, 492
Haghighipour N., Winter O. C., 2016, CeMDA, 124, 235
Haisch K. E., Jr, Lada E. A., Lada C. J., 2001, ApJ, 553, L153
Han E., Wang S. X., Wright J. T., Feng Y. K., Zhao M., Fakhouri O., Brown J. I., Hancock C., 2014, PASP, 126, 827
Hansen B. M. S., Murray N., 2013, ApJ, 775, 53
Horner J., Jones B. W., 2008, Int. J. Astrobiol., 7, 251
Horner J., Jones B. W., 2012, Int. J. Astrobiol., 11, 147
Houtkooper J. M., 2011, Planet. Space Sci., 59, 1107
Ito T., Malhotra R., 2006, Adv. Space Res., 38, 817
Ito T., Tanikawa K., 1999, Icarus, 139, 336
Ito T., Tanikawa K., 2002, MNRAS, 336, 483
Izidoro A., de Souza Torres K., Winter O. C., Haghighipour N., 2013, ApJ, 767, 54
Kominami J., Ida S., 2002, Icarus, 157, 43
Kozai Y., 1962, AJ, 67, 591
Lecar M., Franklin F., 1997, Icarus, 129, 134
Lecar M., Podolak M., Sasselov D., Chiang E., 2006, ApJ, 640, 1115
Lidov M. L., 1962, Planet. Space Sci., 9, 719
Lissauer J. J. et al., 2011, ApJS, 197, 8
Lunine J. I., 2006, in Lauretta D. S., McSween H. Y., Jr, eds, Meteorites and the Early Solar System II, Univ. Arizona Press, Tucson, p. 309
Malhotra R., 1999, Nature, 402, 599
Malhotra R., 2012, Encyclopedia Life Support Syst. UNESCO, 6, 55
Malhotra R., Fox K., Murray C. D., Nicholson P. D., 1989, A&A, 221, 348
Martin R. G., Livio M., 2013, MNRAS, 434, 633
Martin R. G., Livio M., 2015, ApJ, 810, 105
Martin R. G., Livio M., 2016, ApJ, 822, 90
Martin R. G., Lubow S. H., Nixon C., Armitage P. J., 2016, MNRAS, 458, 4345
Michtchenko T. A., Ferraz-Mello S., 2001, Icarus, 149, 357
Minton D. A., Malhotra R., 2010, Icarus, 207, 744
Minton D. A., Malhotra R., 2011, ApJ, 732, 53
Moons M., 1996, Celest. Mech. Dyn. Astron., 65, 175
Morales F. Y., Rieke G. H., Werner M. W., Bryden G., Stapelfeldt K. R., Su K. Y. L., 2011, ApJ, 730, L29
Morbidelli A., Gladman B., 1998, Meteorit. Planet. Sci., 33, 999
Morbidelli A., Nesvorný D., 1999, Icarus, 139, 295
Morbidelli A., Gonczi R., Froeschle C., Farinella P., 1994, A&A, 282, 955
Morbidelli A., Zappala V., Moons M., Cellino A., Gonczi R., 1995, Icarus, 118, 132
Morbidelli A., Chambers J., Lunine J. I., Petit J. M., Robert F., Valsecchi G. B., Cyr K. E., 2000, Meteorit. Planet. Sci., 35, 1309
Morrison S., Malhotra R., 2015, ApJ, 799, 41
Morton T. D., Winn J. N., 2014, ApJ, 796, 47
Murray C. D., Dermott S. F., eds, 2000, Solar System Dynamics. Cambridge Univ. Press, Cambridge, UK
Murray N., Holman M., 1997, AJ, 114, 1246
Murray N., Holman M., 1999, Science, 283, 1877
O'Brien D. P., Morbidelli A., Bottke W. F., 2007, Icarus, 191, 434
Petit J.-M., Morbidelli A., Chambers J., 2001, Icarus, 153, 338
Raymond S. N., Quinn T., Lunine J. I., 2007, Astrobiology, 7, 66
Raymond S. N., O'Brien D. P., Morbidelli A., Kaib N. A., 2009, Icarus, 203, 644
Schlichting H. E., Warren P. H., Yin Q.-Z., 2012, ApJ, 752, 8
Strom R. G., Malhotra R., Ito T., Yoshida F., Kring D. A., 2005, Science, 309, 1847
Takeda G., Rasio F. A., 2005, ApJ, 627, 1001
Valencia D., Sasselov D. D., O'Connell R. J., 2007, ApJ, 665, 1413
Vrbik J., 1996, J. Phys. A: Math. Gen., 29, 3311
Walker R. J., 2009, Chemie der Erde/Geochemistry, 69, 101
Ward W. R., 1989, ApJ, 345, L99
Ward W. R., 1993, Icarus, 106, 274
Willbold M., Elliott T., Moorbath S., 2011, Nature, 477, 195
Wu Y., Murray N., 2003, ApJ, 589, 605
Wyatt M. C., 2003, ApJ, 598, 1321
Yoshikawa M., 1987, Celest. Mech., 40, 233

This paper has been typeset from a TEX/LATEX file prepared by the author.